Chemisorption of H2O and CO2 on hydrotalcites for sorptionenhanced water-gas-shift processes

Available online at www.sciencedirect.com

ScienceDirect

Energy Procedia 114 (2017) 2228 – 2242

Energy Procedia

13th International Conference on Greenhouse Gas Control Technologies, GHGT-13, 14-18 November 2016, Lausanne, Switzerland

Chemisorption of H_2O and CO_2 on hydrotalcites for sorption-enhanced water-gas-shift processes

K. Coenen[a], F. Gallucci[a], P. Cobden[b], E. van Dijk[b], E.J.M. Hensen[a], M. van Sint Annaland[a] *

[a]*Eindhoven University of Technology, 5600 MB Eindhoven, the Netherlands*
[b]*ECN, P.O. Box 1, 1755 ZG Petten, the Netherlands*

Abstract

Thermogravimetric analysis and breakthrough experiments in a packed bed reactor were used to validate a developed adsorption model to describe the cyclic working capacity of CO_2 and H_2O on a potassium-promoted hydrotalcite, a very promising adsorbent for sorption-enhanced water-gas-shift applications. Four different adsorption sites (two sites for CO_2, one site for H_2O and one equilibrium site for both species) were required to describe the mass changes observed in the TGA experiments. The TGA experiments were carried out at operating temperatures between 300 and 500 °C, while the total pressure in the reactor was kept at atmospheric pressure. Cyclic working capacities for different sites and the influence of the operating conditions on the cyclic working capacity were studied using the developed model. A higher operating temperature leads to a significant increase in the cyclic working capacity of the sorbent for CO_2 attributed to the increase in the desorption kinetics for CO_2. The model was successfully validated with experiments in a packed bed reactor at different operating temperatures.

Peer-review under responsibility of the organizing committee of GHGT-13.

* Corresponding author. Tel.: +0-000-000-0000 ; fax: +0-000-000-0000 .
E-mail address: F.gallucci@tue.nl

Peer-review under responsibility of the organizing committee of GHGT-13.
doi:10.1016/j.egypro.2017.03.1360

Keywords: Hydrotalcite; model for cyclic working capacity; CO_2 capture

1. Introduction

Sorption-enhanced water-gas-shift (SEWGS) is a promising concept for pre-combustion CO_2 capture. The water-gas-shift (WGS) and CO_2 removal is combined in a single unit operation enabling high CO conversions at high temperatures (400 °C), which is due to the shift of the WGS equilibrium [1], [2]. It has been demonstrated that SEWGS can reduce the CO_2 capture costs by more than 17% compared to Selexol in an integrated gasification combined cycle (IGCC) power plant [3]. The SEWGS process is a kind of pressure swing adsorption (PSA) based on reversible in situ CO_2 adsorption on a solid material [4]. Typically multiple adsorption columns are operated in parallel at temperatures between 300 and 550 °C.

Hydrotalcite-based adsorbents are suitable candidates for SEWGS because of their fast absorption/desorption kinetics [5], [6], high mechanical stability [7], [8], and high selectivity towards CO_2 compared to CO and H_2. Hydrotalcites are layered double hydroxides (LDH) which belong to the group of anionic clays. The most common stoichiometry for hydrotalcites is the double magnesium-aluminum hydroxide with formula $Mg_6Al_2(HO)_{16}CO_3^{2-}$ x 4 H_2O and the molar ratio of Mg/Al can vary between 1.7 and 4 [9]. Increasing the Mg/Al ratio leads to an increase in basicity, being beneficial for absorption of sour gases such as CO_2 [10]. A good way to further tune the basicity is the promotion of the hydrotalcites with alkaline anions [8]. It has been frequently reported that an impregnation with K_2CO_3 can increase the sorption capacity of CO_2 [6], [11], [12]. For hydrotalcites with higher Mg/Al ratios the formation of $MgCO_3$ has been reported at high partial pressures of steam and CO_2, leading to mechanical stability issues [8], [13]. The initial layered hydrotalcite structure present at room temperature disappears during calcination of the material. Upon heating the material releases CO_2 and H_2O and the original structure changes to a $Mg(Al)O_x$ mixed metal oxide [10], [14]. Typically, hydrotalcites are calcined in air are between 673 and 773 K. When exposed to water and anions, hydrotalcites can reconstruct to the layered structure (memory effect) [15].

The adsorption of CO_2 on different hydrotalcite based adsorbents has been investigated in various studies, since they are available in large quantities and in different chemical compositions which can be used for different applications [16]–[23].

The understanding of the sorbent function can be improved by elucidating the complex behavior involving absorption/desorption phenomena of CO_2 and H_2O from various sites in the adsorbent. It has been reported that steam can increase the CO_2 cyclic adsorption capacity of potassium promoted hydrotalcites, but a full description of the mechanisms involving H_2O and CO_2 on this material is still missing [6], [8], [20], [23].

A complex mechanism involving four different sites to describe the adsorption and desorption behavior of CO_2 and H_2O on a potassium promoted adsorbent has been recently proposed [24]. This paper investigates the influence of the operating conditions on the proposed adsorption sites. Additional thermogravimetric analyses (TGA) and breakthrough experiments in a packed bed reactor were performed varying the inlet gas composition and operating temperature. The obtained data helped improving our insights in the complex mechanism of CO_2 and H_2O adsorption on a hydrotalcite-based adsorbent and validated the developed mechanism also for other operating conditions.

Nomenclature

PBR	Packed Bed Reactor
TGA	Thermogravimetric Analysis

2. Materials and methods

A potassium promoted hydrotalcite based adsorbent with an Mg/Al ratio of 0.54 and a potassium loading of approximately 20 wt.% (supplied in pellet form, 4.7 x 4.7 mm), was crushed to powder and used in the experiments.

The adsorbent will be further denoted as KMG30. The material was characterized using a helium pycnometer (Quantachrome Upyc 1200e), BET (Thermo Fischer Surfer), mercury porosimetry (Thermo Fischer Pascal 140/440), XRD (Rigaku Miniflex 600) and SEM-EDX to study the morphology. Characterization results have already been reported elsewhere [25].

TGA experiments were performed using an in-house designed setup for operation up to 10 bar. A microbalance (Sartorius M25D) with a sensitivity of 1 µg and 200 mg of operating range is connected to a reactor designed for TGA experiments. The maximum operating temperature of this reactor is 1100 °C. A N_2 purge flow is used to purge the balance and the reactor heating elements to avoid reactive gas mixtures damaging either the balance or the heating elements. The gas feeding system with Bronkhorst mass flow controllers (MFC) is capable to produce different reactive gas mixtures. A controlled evaporator mixer (CEM) system is used to produce desired quantities of steam. All lines are traced and can be heated up to 450 °C to avoid steam condensation even at high pressures. A porous ceramic basket was used with approximately 100 mg of sample mass for each experiment. At every pressure, the gas flow rate was adjusted such that mass transfer limitations due to the reduced volumetric flow rate in the reactor are avoided. The measured weight change of all experiments was corrected with a blank experiment containing, which were carried out in the same way as the experiment with an empty basket. A PFD of the used TGA setup is given in Figure 1.

The weight change obtained by TGA experiments to study the cyclic sorption capacity, cannot directly be correlated to specific adsorbing/desorbing species for gas mixtures in case multiple species interact with the material. TGA cycles containing different adsorption and regeneration steps with different gas compositions were designed in order to be able to link the weight change to a certain gas component adsorbed or desorbed. To understand the influence of steam on the adsorption of CO_2, a basic set of experiments was designed and performed in the TGA. The same steam concentration of 34% was chosen as in an earlier study [26]. CO_2 adsorption was measured with a CO_2 partial pressure of 0.66 bar. Each step in the TGA cycle had a duration of 30 min as it was established earlier that a half-cycle time of 30 min is sufficiently high to study the prevailing phenomena in the reactive system [25].

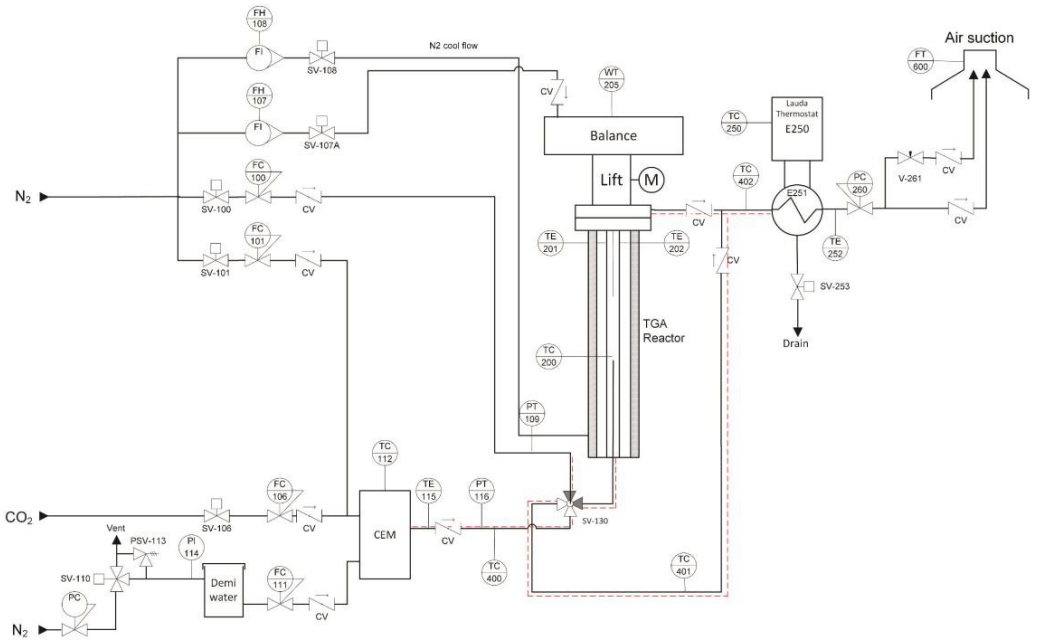

Figure 1 Process Flow Diagram (PFD) of the in-house designed TGA setup

In addition, packed bed reactor experiments were carried out using a small packed bed reactor with a diameter of 27 mm and 350 mm height (AISI 316L). The reactor was filled with 53.6 g of KMG30 with a sieve fraction of 1.8-3.15 mm. The effective length of the packed bed was determined at 176 mm. The reactor was installed in an electrical furnace. A multipoint thermocouple (10 measuring points with a spacing of 20 mm) was installed to measure the axial temperature profile in the bed to observe temperature fronts due to sorption effects. A gas feeding system with Bronkhorst mass flow controllers and a CEM system was used in order to supply the desired gas mixtures including steam. All gas lines to the reactor were traced and heated to avoid steam condensation. The reactor could be bypassed in order to accurately measure the gas composition before exposing the material to the gas mixture. Two independent gas analyzing systems were used to monitor the gas composition in the outlet stream during the experiments. A SICK GMS 800 gas analyzer for CO_2, CO CH_4, H_2 and O_2 was used to monitor the gas composition continuously. In order to measure the steam content in the gas streams an Agilent Technologies Cary 630 FTIR with CaF_2 windows was used together with a RED-SHIFT gas sampling system. The FTIR was calibrated prior to the experiments using the classical Lambert-Beer law in typical adsorption spectra for the gases CO_2, CH_4 and H_2O. CH_4 was used as a tracer gas during the experiments to determine the total gas flow rate in order to convert the measured gas quantities to molar flow rates. It was proved that CH_4 did not show any interaction with the material and was not reacting with steam under the used operating conditions. A total gas flow rate of 0.5 Nl/min was used during the experiments with CO_2, H_2O and CH_4 mole fractions of 0.025, 0.10 and 0.10 respectively (balance N_2). When changing the gas composition, the reactor was bypassed for 5 min while the gas composition was measured. After this stabilization time the feed was sent to the reactor from bottom to top while monitoring the outlet composition of the reactor. Experiments were conducted at atmospheric pressure and 400 °C. The empty volume of the reactor and the tubing was determined previously with blank measurements to correct the breakthrough times for the residence time in both the FTIR and SICK gas analyzers. The reported results in this publication are the results obtained by the FTIR gas analyzer. A process flow diagram of the used setup is given in Figure 2.

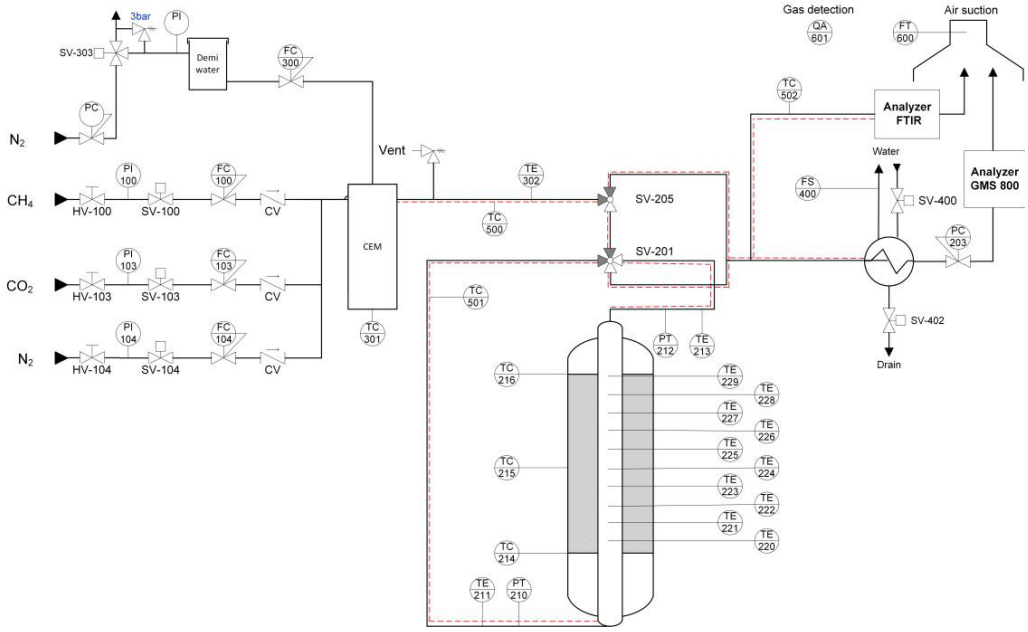

Figure 2 Process Flow Diagram (PFD) of the packed bed reactor (PBR) setup

Table 1 shows an overview of the different experiments performed in the TGA and PBR. One experiment can consist of 2 to 5 different steps. In the table a step is indicated as follows: STEP1 ⇨ STEP2, where the different gas

components in the reactor feed for each step are indicated. Every experiment was performed in cyclic operation, i.e. starting again with the first step after the last step.

Table 1 Different experiments to study the influence of steam on the CO_2 sorption capacity of KMG30

Experiment number	Experimental cycle description	Steps in cycle	Total cycle time (min)
1	$H_2O/N_2 \Rightarrow N_2$	2	60
2	$CO_2 \Rightarrow N_2$	2	60
3	$CO_2 \Rightarrow N_2 \Rightarrow N_2/H_2O \Rightarrow N_2$	4	120
4	$CO_2 \Rightarrow CO_2/H_2O \Rightarrow N_2 \Rightarrow N_2/H_2O \Rightarrow N_2$	5	150
5	$CO_2/H_2O \Rightarrow CO_2 \Rightarrow N_2 \Rightarrow N_2/H_2O \Rightarrow N_2$	5	150
6	$CO_2/H_2O \Rightarrow N_2 \Rightarrow N_2/H_2O \Rightarrow N_2$	4	120
7	$CO_2/H_2O \Rightarrow N_2/H_2O$	2	60
8	$CO_2/H_2O \Rightarrow N_2/H_2O \Rightarrow N_2$	3	90

The experiments were mainly conducted using the TGA since we can directly measure the adsorption kinetics when using pure components in the feed gas stream, having proved the absence of external and internal mass transfer limitations with previous experiments. However, the weight change obtained during the TGA experiments, to study the cyclic sorption capacity, cannot directly be correlated to specific adsorbing/desorbing species for gas mixtures in case multiple species interact with the material. Therefore, additional packed bed reactor experiments were carried out at the same temperature and total pressure. Details on the mechanism of CO_2 and H_2O adsorption on KMG30 using TGA and PBR experiments have been published recently [24]. In this earlier work, we have conducted all experiments in both the TGA and PBR, from which we have learnt that especially experiments 4 and 5 are crucial to understand the adsorption mechanism. Therefore, these experiments were conducted also in the PBR together with experiments 2 and 3. Table 2 shows a summary of the different experiments conducted in both the TGA and PBR. Before each experiment the adsorbent was pre-treated for 2 h at 600 °C with a stream of N_2.

Table 2 Overview of the different experiments conducted in the TGA and PBR

Setup	Temperature (°C)	P CO_2 (bar)	P H_2O (bar)	P CH_4 (bar)	Experiments	Number of cycles
TGA	300	0.66	0.34	-	1-8	5
TGA	400	0.66	0.34	-	1-8	5
TGA	500	0.66	0.34	-	1-8	5
PBR	300	0.025	0.1	0.1	2-5	2
PBR	400	0.025	0.1	0.1	2-5	2
PBR	500	0.025	0.1	0.1	2-5	2

3. Results & Discussion

3.1. TGA experiments for CO_2 and H_2O at different operating temperature

The normalized weight change for the adsorption and desorption of CO_2 and H_2O conducted with TGA are plotted in Figure 3. The gases fed to the reactor are indicated together with the change in gas feed in order to visualize the start and end of one adsorption/desorption step. From Figure 3a it is clear that the weight increase during the adsorption of CO_2 hardly depends on the operating temperature. However, the weight decrease during the desorption of CO_2 is strongly temperature dependent, showing a much faster and increased weight loss at higher operating temperatures. During the second adsorption step the same final weight is reached for the different operating temperatures, however at a somewhat higher weight change than after the first adsorption step. From these experiments it can be concluded that the CO_2 sorption capacity of KMG30 does not depend on the operating temperature. Small differences in the adsorption kinetics can be discerned during the first adsorption step, but are almost negligible during the second adsorption step with CO_2. However, the desorption rate of CO_2 is strongly enhanced when the temperature is increased. A higher operating temperature usually enables the desorption of stronger chemisorbed species, which can explain the obtained results.

Figure 3b shows the weight change of the sample during the adsorption of H_2O on the same adsorbent at different operating temperatures using 0.34 bar of H_2O. The figure shows that for the adsorption of H_2O the highest weight increase is obtained at the lowest temperature, contrary to the CO_2 adsorption. At 500 °C a slow weight decrease is observed after the initial fast adsorption. During the desorption step with N_2 part of the initially gained weight is lost. After the second adsorption step the same weight is reached as during the first adsorption step. For H_2O the operating temperature has a significant influence on the adsorption capacity of the adsorbent. At higher temperatures the adsorbent takes up significantly smaller amounts of H_2O. The small weight decrease at 500 °C after the fast initial weight increase is probably caused by further desorption of CO_2 due to the presence of H_2O. We have reported earlier that the adsorbent releases especially CO_2 at higher temperatures, whereas H_2O is already desorbed at lower temperatures [25]. Even though the adsorbent was pre-treated at 600 °C for 120 min, CO_2 can be released at high temperatures upon exposure of the sorbent to H_2O. Similarly as obtained for CO_2, during the desorption step not all the H_2O that was previously adsorbed can be desorbed especially at lower temperatures, whereas at 500 °C the weight loss is nearly the same as the weight gain during the adsorption.

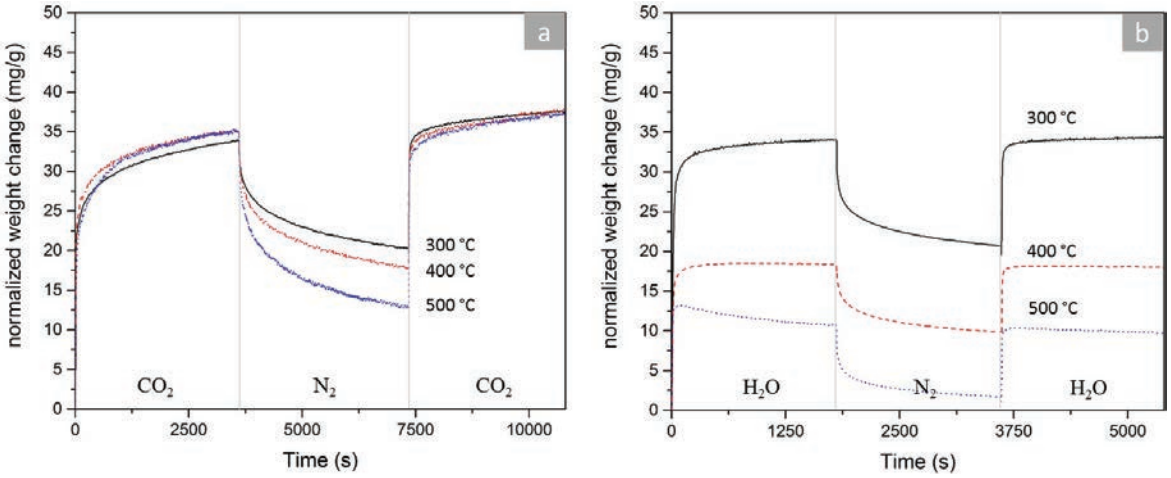

Figure 3 a) CO_2 adsorption at different temperatures at PCO_2 = 1 bar b) Adsorption and desorption of H_2O at PH_2O = 0.34 bar

Since the SEWGS requires cyclic operation, the cyclic working capacity of the adsorbent is one of the most important properties. The cyclic working capacity is defined as the average of the amount of sorbate adsorbed and desorbed with respect to the sample weight after the pre-treatment. The cyclic working capacity for both CO_2 and H_2O at different operating temperatures is shown in Figure 4. The results clearly show that a higher operating temperature leads to an increase in the cyclic working capacity for CO_2 but to a decrease in the cyclic working capacity for H_2O. For CO_2, the cyclic working capacity is mainly determined by the desorption step, since the CO_2 desorption rate is much slower compared to the CO_2 adsorption rate. An increase in temperature strongly increases the desorption rate and hence the cyclic working capacity. For H_2O the cyclic working capacity is especially determined by the adsorption step, where an increase in the operating temperature leads to a significant decrease in the amount of H_2O that can be adsorbed, and hence in the cyclic working capacity. It should to be noted that in general the desorption rate is slower, so that an increase in desorption time (cycle time) leads to an increase in the cyclic working capacity for both CO_2 and H_2O, as reported earlier [25].

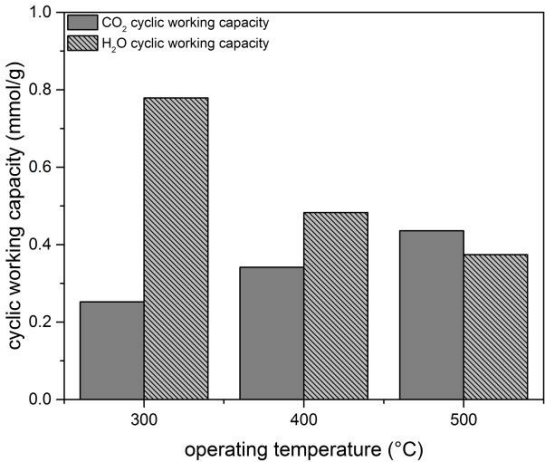

Figure 4 Cyclic working capacity for CO_2 and H_2O of KMG30 at different operating temperatures (PCO_2 = 1bar, PH_2O = 0.34 bar)

3.2. Model for CO_2 and H_2O adsorption on KMG30

We have published recently a mechanism which can describe the adsorption and desorption of both CO_2 and H_2O on KMG30 [24]. This mechanism is based on experiments with both the TGA and PBR at 400 °C and involves four different adsorption sites. Table 3 provides a summary of the different sites involved in the proposed mechanism for CO_2 and H_2O adsorption on KMG30. The cyclic working capacities reported in this table were determined at 400 °C and PH_2O = 0.34 bar and PCO_2 = 0.66 bar. A detailed description and the development of the mechanism has been reported elsewhere [24]. Summarizing the results, we have found that the KMG30 has one site for H_2O (site A), which can be regenerated with N_2. The results for H_2O adsorption at different temperatures discussed in the previous section refer to adsorption of H_2O on this site. Site B is a site for CO_2 which can be regenerated with N_2 and it is assumed that CO_2 is relatively weakly bonded to the adsorbent. The cyclic working capacity of this site at different temperatures was also discussed in the previous section.

Site C is a site which can be either occupied with CO_2 or H_2O. If both gases are fed to the adsorbent an equilibrium will be established between CO_2 and H_2O (site C_{eq} in Table 3). Once site C is occupied by either H_2O or CO_2 (dependent on which species was fed to adsorbent first) it can only be regenerated by a replacement with the other gaseous species. If for example the adsorbent was exposed to a dry gas stream containing CO_2 first, H_2O is required to desorb the CO_2 adsorbed on site C.

If CO_2 and H_2O are fed simultaneously to the adsorbent additionally to the established equilibrium between CO_2 and H_2O on site C, the adsorbent can adsorb an additional amount of CO_2 which is related to adsorption of CO_2 on site D. It is only active after both CO_2 and H_2O are used together in an adsorption step (e.g. EXP4 in Table 1). CO_2 from this site can be regenerated fully with H_2O or only partly with N_2 if the material was exposed previously to H_2O and is still wet (e.g. desorption step with N_2 after a step with CO_2/H_2O). Based on this mechanism a simple model was developed to be able to describe the cyclic working capacity for CO_2 and H_2O in each experimental step according to the conditions mentioned. This model is further validated with the experiments described in the next paragraph.

Table 3 Mechanism for CO_2 and H_2O adsorption on KMG30

Site	Adsorbate	regeneration conditions	cyclic working capacity mg/g	cyclic working capacity mmol/g	description
A	H_2O	dry	5	0.28	always
B	CO_2	dry	12	0.3	always (increased capacity after first time CO_2/H_2O)
D	CO_2	wet	6	0.14	activated after first time CO_2/H_2O
C	H_2O	CO_2	7.5	0.42	H_2O feed
	CO_2	H_2O	18.5	0.42	dry CO_2 feed
C_{eq}	CO_2	H_2O	4.5	0.1	CO_2/H_2O feed
	H_2O	CO_2	5.7	0.32	

3.3. Validation of mechanism with TGA experiments

Experiments were conducted in the TGA using different operating temperatures and different CO_2 partial pressures (see Table 2). The cyclic mass change was determined for each step in an experiment. The cyclic average mass change of the last three experiments (out of 5) are plotted for all experiments in the appendix. The cyclic working capacity of each site according to the mechanism introduced previously was fitted using the developed model. The resulting cyclic working capacity determined for each sites are given in Table 4, whereas the resulting deviation and the total deviation (all in mg/g) can be found together with the experimental results in the appendix. Considering that the maximum deviation of our model with the experimental data is between 0.44 and 0.79 mg/g (i.e. in the order of the experimental error), it can be concluded that the model is able to predict the experimental results quite adequately.

Table 4 Fitting Results of 4 Site model to experimental Data

NO	Temperature (°C)	P CO_2 (bar)	P H_2O (bar)	Fitting Results of Model				
				A	B	C	C_{eq}	D
1	300	0.66	0.34	9.72	9.05	10.93	4.12	4.93
2	400	0.66	0.34	8.28	10.71	11.76	5.55	5.44
3	500	0.66	0.34	6.34	11.00	11.54	5.59	5.26

Figure 5a shows the cyclic working capacity of the different adsorption sites at different operating conditions. It can be seen that the cyclic working capacity of site A (H_2O) indeed decreases at higher temperatures (lower amount of H_2O adsorbed), confirming results reported before. The cyclic working capacity of site B (CO_2) increases at higher temperatures (increased desorption rate). The cyclic working capacity of site C and C_{eq} both seem to increase somewhat at higher operating temperatures, whereas the cyclic working capacity of site D remains basically constant. The slight increase in the cyclic working capacity of site C could also be explained with faster desorption kinetics of this site, but the kinetics of this site cannot be obtained directly from the TGA experiments (due to simultaneous adsorption and desorption of two gaseous species). The small cyclic working capacity increase of site C_{eq} can be caused by a decrease in the amount of H_2O sorption at higher operating temperatures, thus shifting the equilibrium of this site towards CO_2. Since the molar mass of CO_2 is higher than H_2O, the cyclic working capacity in mg/g is increased if the equilibrium is shifted towards the adsorption of CO_2.

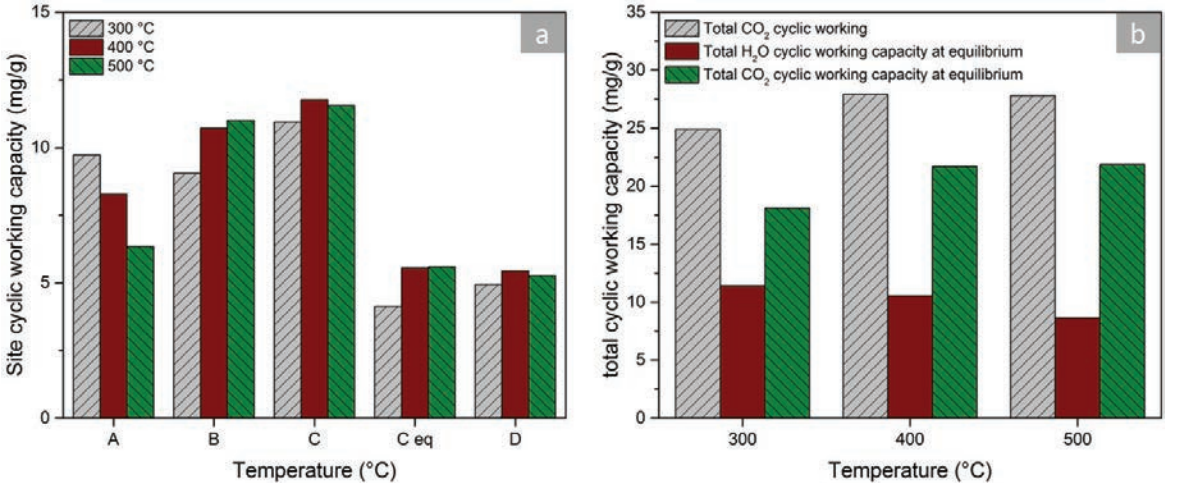

Figure 5 a) Cyclic working capacity of the different sites at different operating temperatures; b) total cyclic working capacity for CO_2 and H_2O as a function of the operating temperature

The changes in cyclic working capacity of the different adsorption sites at different operating temperatures leads to a change in the total adsorption capacity of the adsorbent for a cyclic operation, shown in Figure 5b. The total cyclic working capacity for CO_2 is both increased when operating at equilibrium (CO_2 and H_2O fed simultaneously) or at dry conditions, where the cyclic working capacity for CO_2 is higher for dry CO_2 gas streams. For H_2O the total cyclic working capacity at equilibrium is decreased when the operating temperature is increased.

3.4. Validation of model with PBR experiments

For the breakthrough results obtained with the packed bed reactor the response of the FTIR analyzer is plotted (vol%) as a function of time, using the graphical representation explained in Figure 6. The signal for CO_2 and the corresponding areas (integration of analyzer signal over time with respect to the baseline) are plotted in red, whereas the signal and areas for H_2O are plotted in blue. We distinguish between adsorption (solid area below the signal) and desorption (shaded area above the analyzer signal).

Figure 6 Graphical representation of packed bed reactor experiments

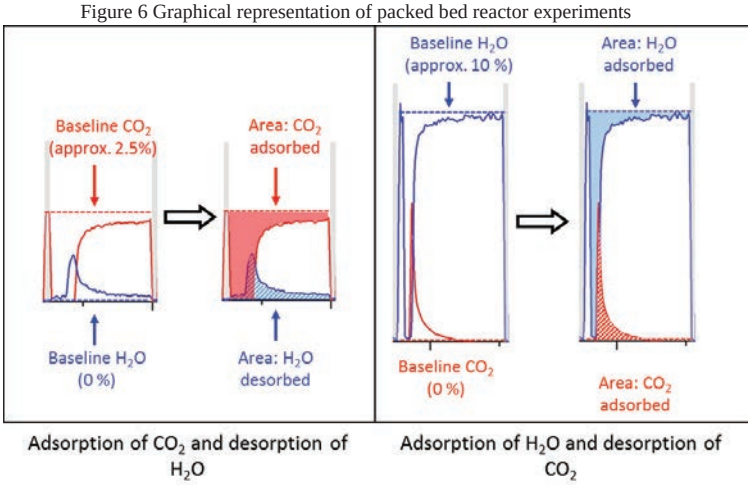

The results for the different breakthrough experiments performed in the packed bed reactor (PBR) are plotted in the Figure 7, showing the concentration profiles for CO_2 and H_2O together with the temperature at three different axial positions in the bed at 1, 5 and 9 cm from the inlet. For experiments 2 and 3 (Figure 7a and b) both cycles of the experiments are plotted, where we only plot one cycle for the experiments 4 and 5 (Figure 7c and d) for clarity. Figure 8a shows the concentration and temperature profiles for the first and second adsorption cycle of CO_2 followed by a desorption step with N_2. The CO_2 breakthrough time during the first cycle is longer (corresponding to a higher CO_2 adsorption capacity) compared to the second cycle, whereas the amount of CO_2 desorbed in both cycles are similar. During the first adsorption cycle a temperature rise of about 10 °C at different adsorption times is measured, while the temperature rise is much lower (only about 3 °C) during the second adsorption cycle. Note that when N_2 is fed to the reactor (desorption of CO_2) the temperature remains almost constant in the reactor.

The first part (step 1 and 2) of experiment 3 is similar to the second cycle of experiment 2 and the same results are obtained. In step 3 the sorbent is exposed to H_2O and during the adsorption of H_2O, CO_2 is simultaneously desorbing while a temperature peak of about 11 °C is observed. Note that the breakthrough of CO_2 is not occurring directly at the beginning of the step. In step 4 (N_2) part of the H_2O is desorbing together with a small decrease in the bed temperature. During the subsequent step (CO_2) the amount of CO_2 that is adsorbed is increased (longer breakthrough time), while simultaneously H_2O is desorbing, and the breakthrough of H_2O does not occur directly at the beginning of this step (similar as for CO_2 in step 3). Steps 6 – 8 show the same behavior for both concentration and temperature profiles as observed for steps 3 – 4. Both the temperature rise and the adsorption capacity for H_2O in step 7 are slightly lower compared to those for step 3.

In experiment 4 we started with a dry adsorption of CO_2 (equal to experiment 3, step 5) and the obtained profiles are the same. If we introduce CO_2/H_2O in step 2 we can obtain a temperature rise in the reactor together with adsorption of H_2O and direct desorption of CO_2. In step 3 both CO_2 and H_2O are desorbing with a temperature drop in the bed (simultaneous breakthrough of CO_2 and H_2O). In step 4 H_2O is adsorbed with a temperature rise in the bed and CO_2 is desorbed, whereas the CO_2 breakthrough is somewhat later. In the step 5 only H_2O is released by the sorbent together with a temperature drop similar to step 3.

Figure 7d shows the concentration and temperature profiles of experiment 5. During step 1 both CO_2 and H_2O adsorb and the temperature in the reactor increases. After the sharp breakthrough of H_2O, the measured concentration is higher than the feed concentration (indicating desorption of H_2O). During step 2 H_2O is desorbing and additional CO_2 is adsorbed by the sorbent . Only a moderate temperature decrease is observed during this step. In step 3 mainly CO_2 is desorbing with a constant bed temperature during this step (similar to step 6 in Figure 7b). The concentration and temperature profiles in steps 4 and 5 are similar to steps 7 and 8 in the Figure 7b.

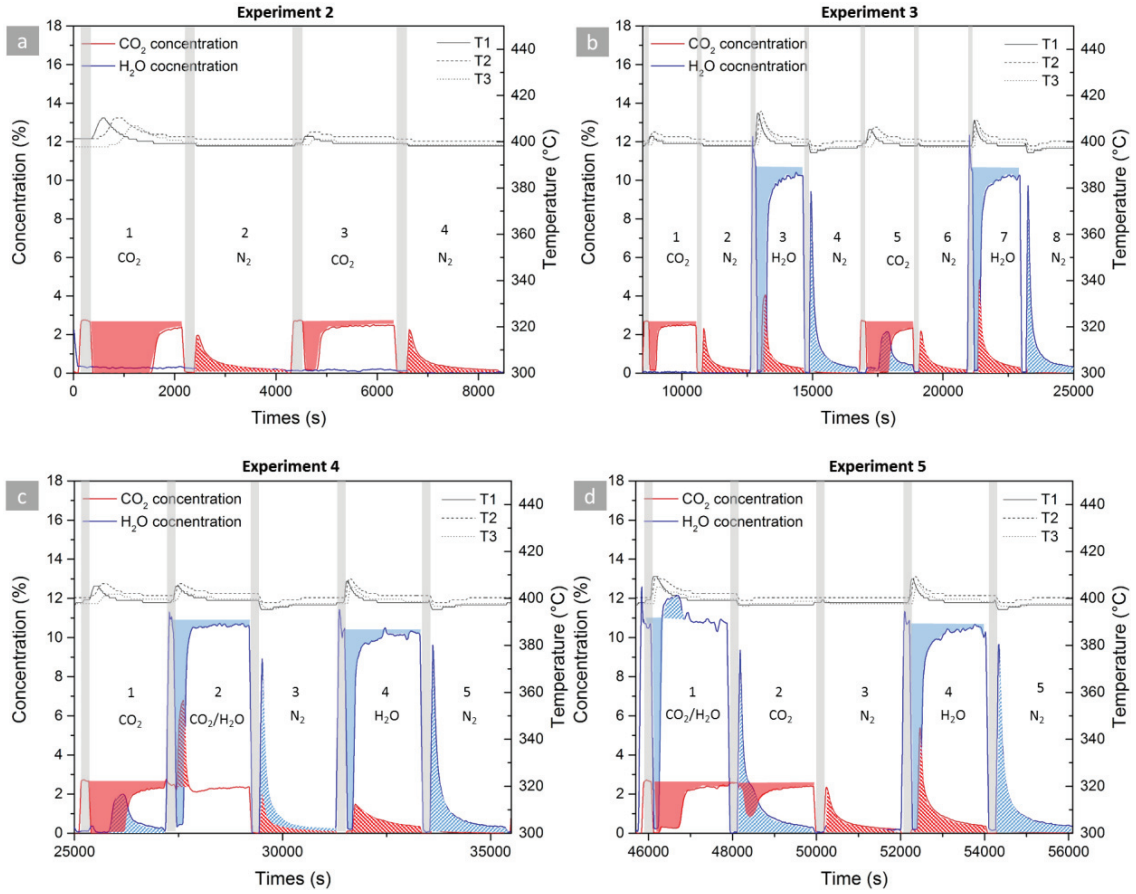

Figure 7 Concentration profiles of CO_2 and H_2O and Temperature profiles for T1, T2, T3 at 1, 5, 9 cm bed height for PBR experiments at 400°C PCO_2=0.025 bar PH_2O=0.1 bar a) EXP2 b) EXP3 c) EXP4 d) EXP5

The results obtained from these experiments confirm the earlier described mechanism. During the first cycle all available sites are covered by CO_2 resulting in a high CO_2 adsorption capacity with a significant temperature rise indicating that the adsorption of CO_2 is an exothermic process. However during the subsequent desorption of CO_2 with N_2 only a very small temperature decrease is observed. This is caused by the slow desorption kinetics of CO_2 and only one site of CO_2 being desorbed with N_2 (Site B). During the second adsorption cycle of CO_2 (experiment 2, step 3) site B is covered again with CO_2 which was desorbed in the previous step resulting in a relatively low CO_2 adsorption capacity and only a moderate temperature increase in the bed.

During step 3 in experiment 3 (Figure 7b) site C and A are covered by H_2O where the CO_2 adsorbed previously on site C is desorbed. That steam can enhance the desorption of CO_2 from potassium promoted hydrotalcites has been reported in the literature before [27]. It can be seen that this process leads to a significant temperature increase in the reactor probably related to the adsorption of H_2O. This is confirmed in the next step where the desorption of H_2O leads to a temperature decrease in the reactor which is significantly higher compared to the desorption of CO_2 (c.f. step 2 of experiment 3). In step 5 CO_2 is adsorbing on both sites C and B while H_2O is replaced by CO_2 which is visible in the late breakthrough of H_2O. Because of the higher amount of CO_2 being adsorbed during this step the obtained temperature rise is higher. Due to the simultaneous endothermic desorption of H_2O the temperature rise is smaller. The measured adsorption capacity for H_2O and the measured temperature rise in step 7 are somewhat smaller compared to the those during step 3. It is known, as already reported for CO_2, that some H_2O is irreversibly adsorbed

(under these operating conditions), which is the reason for the obtained results. This is confirmed when comparing step 8 to step 4, where identical concentration and temperature profiles can be seen.

The existence of the equilibrium concentration of site C is proved with experiments 4 and 5. In step 2 of experiment 4, where H_2O is added to the gas stream (note that the partial pressure of CO_2 was kept constant), part of the CO_2 adsorbed on site C is replaced by H_2O. The obtained temperature rise in the reactor is smaller than expected for the adsorption of H_2O (c.f. experiment 3), indicating that the replacement is probably an endothermic process. In the next step CO_2 is desorbed from site B and H_2O from site A. The obtained temperature profile is identical to step 8 in experiment 8, confirming our observation from experiment 2, that the desorption of CO_2 in N_2 does not lead to a significant temperature drop in the bed. Since site C is only partly covered by CO_2 after step 2, the amount of CO_2 desorbed in step 4 is smaller than the amount desorbed in step 7 in experiment 3. In experiment 5 the replacement effect is visible in both steps 1 and 2. During step 1 site A is covered by H_2O and site B by CO_2. Because site C was fully covered by H_2O in the previous step, H_2O is desorbing from this site leading to an increase in the measured H_2O outlet concentration. In step 2 site C is fully covered by CO_2 leading to an additional uptake of CO_2 while replacing H_2O. Additionally, H_2O desorbs from site A which results in an increased amount of H_2O being desorbed during this step compared to e.g. step 3 in experiment 4 where only H_2O from site A desorbs.

These results confirm the developed mechanism for CO_2 and H_2O. Based on the relatively low temperature change in the reactor during the adsorption and desorption of site B it is confirmed that the bond between CO_2 and this site is relatively weak. Replacement of H_2O by CO_2 and desorption of H_2O from the site B result in a stable temperature profile in the reactor, indicating that the adsorption of CO_2 on site C has to be more exothermic, which corresponds to a stronger bonding of CO_2 to site C compared to site B.

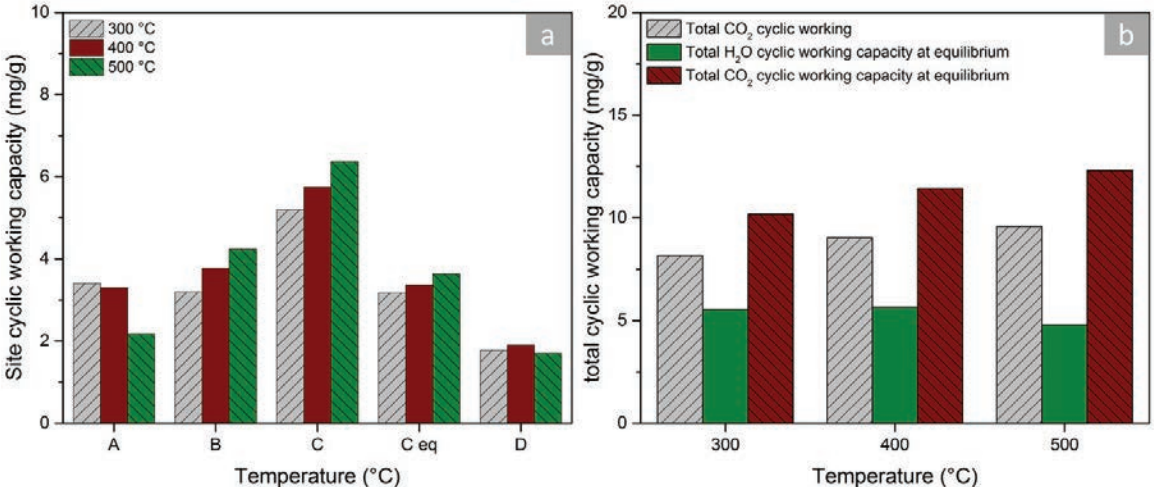

Figure 8 a) Cyclic working capacities for the different sites at different temperatures b) Total cyclic working capacities for CO_2 and H_2O on KMG30 at different temperatures

Figure 8a shows the cyclic working capacity of the different sites at three different temperatures, which were calculated from the breakthrough results in the packed bed reactor. It is found that the cyclic working capacity of CO_2 on sites B, C and C_{eq} increase with increasing temperature, whereas the cyclic working capacity of H_2O on site A decreases at higher operating temperatures. The cyclic working capacity of site D hardly depends on the operating temperature. The total cyclic working capacity for both CO_2 and H_2O at different operating temperatures is shown in Figure 8b. It can be seen that the cyclic working capacity of the sorbent is increased at higher operating temperatures both for dry CO_2 feed and also at equilibrium (CO_2/H_2O feed). The cyclic working capacity for H_2O is slightly decreased at higher operating temperatures.

Comparing these results to the results obtained from the TGA experiments described in section 3.3 (see Figure 5) it can be concluded that the same influences of the operating temperature on the total cyclic working capacity for CO_2 and H_2O are found with both experimental techniques, although the absolute values are somewhat different because

of the different operating conditions. Where with the TGA it can be assumed that the adsorbent is exposed to a constant gas phase concentration, in the packed bed reactor moving concentration fronts makes it difficult to compare absolute cyclic working capacities, even when operating at the same feed concentration and adsorption/desorption times. However, both techniques show the same trend as a function of the operating temperature supported the prosed adsorption mechanism.

4. Conclusions

We have shown with TGA experiments, that the adsorption mechanism and the influence of the operating temperature on the adsorption of CO_2 and H_2O is different. A higher operating temperature leads to an increase in the desorption kinetics for CO_2 thereby increasing the cyclic working capacity for CO_2. For H_2O the adsorption capacity is decreased at higher temperature resulting in a lower cyclic working capacity at higher temperatures.

We have shown with both TGA and PBR experiments that the already developed mechanism with four different adsorption sites (two sites for CO_2, one site for H_2O and one equilibrium site for both species) can well describe the amount of adsorbed CO_2 and H_2O on a potassium promoted hydrotalcite at different operating temperatures, enabling a description of the cyclic working capacities of the different sites involved at different operating conditions. The developed model was validated with experiments in a packed bed reactor system at different operating temperatures. It could be proved that a change in the operating temperature indeed influences the cyclic working capacity of the different sites and the model based on TGA experiments could describe these changes for both experimental techniques.

Appendix

PCO_2 = 0.66 bar PH_2O = 0.34 bar T = 300°C						Model Deviation (mg/g)					
No	CO_2	CO_2/H_2O	N_2	N_2/H_2O	N_2	CO_2	CO_2/H_2O	N_2	N_2/H_2O	N_2	Total deviation (mg/g)
1				10.69	-10.40				0.68	0.48	
2	10.43		-9.33			0.97		0.20			
3	20.74		-10.55	0.61	-9.57	0.54		1.06	1.29	0.11	
4	-2.94	30.89	-12.53	-3.70	-10.12	0.02	1.46	0.01	0.02	0.28	0.680
5	21.65	8.03	-16.63	-2.49	-9.85	0.47	0.13	2.22	2.24	0.09	
6		28.79	-16.56	-2.01	-9.71		0.02	2.27	1.89	0.01	
7		17.60		-17.29			0.35		0.57		
8		27.34		-17.27	-9.77		0.35		0.59	0.03	
PCO_2 = 0.66 bar PH_2O = 0.34 bar T = 400°C						Model Deviation (mg/g)					
No	CO_2	CO_2/H_2O	N_2	N_2/H_2O	N_2	CO_2	CO_2/H_2O	N_2	N_2/H_2O	N_2	Total deviation (mg/g)
1				7.90	-8.06				0.27	0.15	
2	11.57		-10.71			0.60		0.00			
3	22.96		-12.30	-2.12	-7.85	0.34		1.12	3.20	0.31	
4	-1.95	33.72	-15.17	-6.48	-8.51	0.09	1.94	0.52	0.20	0.17	0.567
5	24.94	7.69	-19.27	-4.20	-8.32	1.03	0.12	0.51	1.05	0.03	
6		31.34	-18.91	-3.72	-8.20		0.25	0.76	0.71	0.06	
7		21.71		-21.29			0.71		0.29		
8		30.27		-21.23	-8.35		0.51		0.34	0.05	
PCO_2 = 0.66 bar PH_2O = 0.34 bar T = 500°C						Model Deviation (mg/g)					
No	CO_2	CO_2/H_2O	N_2	N_2/H_2O	N_2	CO_2	CO_2/H_2O	N_2	N_2/H_2O	N_2	Total deviation (mg/g)
1				9.94	-9.81						
2	15.36		-13.94			3.08		2.08			
3	22.92		-12.49	-4.50	-6.44	0.26		1.05	0.50	0.07	
4	-0.45	33.05	-15.49	-8.76	-6.89	0.04	3.44	1.31	0.54	0.39	0.468
5	24.72	5.65	-17.43	-5.83	-6.61	1.54	0.00	0.06	0.93	0.19	
6		28.65	-16.74	-5.23	-6.44		0.32	0.43	0.51	0.07	
7		20.53		-20.31			0.94		1.09		
8		26.45		-20.05	-6.20		1.23		1.27	0.10	

Acknowledgements

The research leading to these results has received support through the ADEM innovation lab program .

References

[1] M. Gazzani, E. MacChi, and G. Manzolini, “CO2 capture in integrated gasification combined cycle with SEWGS - Part A: Thermodynamic performances,” *Fuel*, vol. 105, pp. 206–219, 2013.

[2] J. Boon, V. Spallina, Y. van Delft, and M. van Sint Annaland, “Comparison of the efficiency of carbon dioxide capture by sorption-enhanced water–gas shift and palladium-based membranes for power and hydrogen production,” *Int. J. Greenh. Gas Control*, vol. 50, pp. 121–134, 2016.

[3] G. Manzolini, E. MacChi, and M. Gazzani, “CO2 capture in Integrated Gasification Combined Cycle with SEWGS - Part B: Economic assessment,” *Fuel*, vol. 105, pp. 220–227, 2013.

[4] E. R. van Selow, P. D. Cobden, H. a. J. van Dijk, S. Walspurger, P. a. Verbraeken, and D. Jansen, “Qualification of the ALKASORB sorbent for the sorption-enhanced water-gas shift process,” *Energy Procedia*, vol. 37, pp. 180–189, 2013.

[5] K. B. Lee, a Verdooren, H. S. Caram, and S. Sircar, “Chemisorption of carbon dioxide on potassium-carbonate-promoted hydrotalcite.,” *J. Colloid Interface Sci.*, vol. 308, no. 1, pp. 30–9, Apr. 2007.

[6] E. L. G. Oliveira, C. a. Grande, and A. E. Rodrigues, “CO2 sorption on hydrotalcite and alkali-modified (K and Cs) hydrotalcites at high temperatures,” *Sep. Purif. Technol.*, vol. 62, pp. 137–147, 2008.

[7] A. D. Ebner, S. P. Reynolds, and J. A. Ritter, “Understanding the Adsorption and Desorption Behavior of CO 2 on a K-Promoted Hydrotalcite-like Compound (HTlc) through Nonequilibrium Dynamic Isotherms,” vol. 50, pp. 6387–6392, 2006.

[8] S. Walspurger, P. D. Cobden, O. V Safonova, Y. Wu, and E. J. Anthony, “High CO(2) storage capacity in alkali-promoted hydrotalcite-based material: in situ detection of reversible formation of magnesium carbonate.,” *Chemistry*, vol. 16, no. 42, pp. 12694–700, Nov. 2010.

[9] W. T. Reichle, “Catalytic Reactions by Thermally Activated , Synthetic , Anionic Clay Minerals,” vol. 557, pp. 547–557, 1985.

[10] D. P. Debecker, E. M. Gaigneaux, and G. Busca, “Exploring, tuning, and exploiting the basicity of hydrotalcites for applications in heterogeneous catalysis.,” *Chemistry*, vol. 15, no. 16, pp. 3920–35, Jan. 2009.

[11] N. N. A. H. Meis, J. H. Bitter, and K. P. De Jong, “On the Influence and Role of Alkali Metals on Supported and Unsupported Activated Hydrotalcites for CO2 Sorption,” no. x, pp. 8086–8093, 2010.

[12] S. Walspurger, L. Boels, P. D. Cobden, G. D. Elzinga, W. G. Haije, and R. W. van den Brink, “The crucial role of the K+-aluminium oxide interaction in K+-promoted alumina- and hydrotalcite-based materials for CO2 sorption at high temperatures.,” *ChemSusChem*, vol. 1, no. 7, pp. 643–50, Jan. 2008.

[13] E. R. Van Selow, P. D. Cobden, a. D. Wright, R. W. Van Den Brink, and D. Jansen, “Improved sorbent for the sorption-enhanced water-gas shift process,” *Energy Procedia*, vol. 4, pp. 1090–1095, Jan. 2011.

[14] W. Reichle, S. Kang, and D. Everhardt, “The nature of the thermal decomposition of a catalytically active anionic clay mineral,” *J. Catal.*, no. 7, pp. 352–359, 1986.

[15] D. Tichit, C. Gérardin, R. Durand, and B. Coq, “Layered double hydroxides: Precursors for multifunctional catalysts,” *Top. Catal.*, vol. 39, no. 1–2, pp. 89–96, 2006.

[16] E. R. Van Selow, P. D. Cobden, P. a Verbraeken, J. R. Hufton, and R. W. Van Den Brink, “Carbon Capture by Sorption-Enhanced Water - Gas Shift Reaction Process using Hydrotalcite-Based Material,” pp. 4184–4193, 2009.

[17] P. D. Cobden, P. van Beurden, H. T. J. Reijers, G. D. Elzinga, S. C. a. Kluiters, J. W. Dijkstra, D. Jansen, and R. W. van den Brink, “Sorption-enhanced hydrogen production for pre-combustion CO2 capture: Thermodynamic analysis and experimental results,” *Int. J. Greenh. Gas Control*, vol. 1, no. 2, pp. 170–179, Apr. 2007.

[18] J. Boon, P. D. Cobden, H. a. J. van Dijk, and M. van Sint Annaland, “High-temperature pressure swing adsorption cycle design for sorption-enhanced water–gas shift,” *Chem. Eng. Sci.*, vol. 122, pp. 219–231, Jan. 2015.

[19] E. van Dijk, S. Walspurger, P. Cobden, and R. van den Brink, “Testing of hydrotalcite based sorbents for CO2 and H2S capture for use in sorption enhanced water gas shift,” *Energy Procedia*, vol. 4, pp. 1110–1117, 2011.

[20] M. H. Halabi, M. H. J. M. de Croon, J. van der Schaaf, P. D. Cobden, and J. C. Schouten, “High capacity potassium-promoted hydrotalcite for CO2 capture in H2 production,” *Int. J. Hydrogen Energy*, vol. 37, no. 5, pp. 4516–4525, Mar. 2012.

[21] J. Boon, P. D. Cobden, H. a J. van Dijk, C. Hoogland, E. R. van Selow, and M. van Sint Annaland, “Isotherm model for high-temperature, high-pressure adsorption of CO2 and H2O on K-promoted hydrotalcite,” *Chem. Eng. J.*, vol. 248, pp. 406–414, 2014.

[22] H. T. J. Reijers, S. E. a Valster-Schiermeier, P. D. Cobden, and R. W. Van Den Brink, “Hydrotalcite as CO2 sorbent for sorption-enhanced steam reforming of methane,” *Ind. Eng. Chem. Res.*, vol. 45, no. July, pp. 2522–2530, 2006.

[23] M. Maroño, Y. Torreiro, and L. Gutierrez, “Influence of steam partial pressures in the CO2 capture capacity of K-doped hydrotalcite-based sorbents for their application to SEWGS processes,” *Int. J. Greenh. Gas Control*, vol. 14, pp. 183–192, 2013.

[24] K. Coenen, F. Gallucci, P. Gianmaria, P. Cobden, E. van Dijk, E. Hensen, and M. van Sint Annaland, “On the influence of steam on CO2 chemisorption capacity of hydrotalcite bases adsorbents for SEWGS applications,” *Submitted*, 2016.

[25] K. Coenen, F. Gallucci, P. Cobden, E. van Dijk, E. Hensen, and M. van S. Annaland, “Chemisorption working capacity and kinetics of CO2 and H2O of hydrotalcite-based adsorbents for sorption-enhanced water-gas-shift applications,” *Chem. Eng. J.*, vol. 293, pp. 9–23, 2016.

[26] E. van Dijk, S. Walspurger, P. D. Cobden, R. W. van den Brink, and F. G. de Vos, “Testing of hydrotalcite-based sorbents for CO2 and H2S capture for use in sorption enhanced water gas shift,” *Int. J. Greenh. Gas Control*, vol. 5, pp. 505–511, 2011.

[27] H. T. J. Reijers, S. E. a Valster-Schiermeier, P. D. Cobden, and R. W. Van Den Brink, “Hydrotalcite as CO 2 Sorbent for Sorption-Enhanced Steam Reforming of Methane,” *Ind. Eng. Chem. Res.*, vol. 45, no. 8, pp. 2522–2530, 2006.